Applied Acoustics 184 (2021) 108367

Contents lists available at ScienceDirect

Applied Acoustics

journal homepage: www.elsevier.com/locate/apacoust

Experimental evaluation of targeting accuracy of ultrasound imaging-guided robotic HIFU ablative system for the treatment of solid tumors in pre-clinical studies

Ł. Fura [a], W. Dera [b], C. Dziekoński [b], M. Świątkiewicz [c], T. Kujawska [a,*]

[a] Department of Ultrasound, Institute of Fundamental Technological Research Polish Academy of Sciences, Pawińskiego 5b, Warsaw, Poland
[b] Department of Theory of Continuous Media and Nanostructures, Institute of Fundamental Technological Research Polish Academy of Sciences, Pawińskiego 5b, Warsaw, Poland
[c] Department of Experimental Pharmacology, Mossakowski Medical Research Centre Polish Academy of Sciences, Pawińskiego 5, Warsaw, Poland

ARTICLE INFO

Article history:
Received 1 May 2021
Received in revised form 21 July 2021
Accepted 14 August 2021

Keywords:
Robotic HIFU ablative device
Ultrasound imaging guidance
ex vivo tissues
Necrotic lesions
Targeting accuracy

ABSTRACT

We have designed and built low-cost compact ultrasound imaging-guided robotic HIFU (High-Intensity Focused Ultrasound) ablation device for thermal damage of solid tumors in small animals. Before this device is used to treat animals, experimental studies on *ex vivo* tissues were necessary to assess the accuracy of its targeting, ensuring the safety of therapy. The objective of this study was to assess the targeting accuracy of our device in the focal and axial plane of the HIFU beam using *ex vivo* tissue embedded in a reference cylindrical chamber inside which a coaxial cylindrical volume with a smaller diameter was ablated. HIFU beams with selected acoustic parameters, generated by a singe-element bowl-shaped 64-mm HIFU transducer operating at 1.08 MHz or 3.21 MHz frequency, were propagated in two-layer media: water-tissue (50 mm-40 mm) and focused at 12.6-mm depth below the tissue surface. Cylindrical necrotic lesions of various size were created by moving the chamber using a computer-controlled precise positioning unit. Lesions formed were compared with those intended for treatment using various visualization methods and displacement between their centers were determined. The targeting accuracy in the focal and axial planes was found to be respectively about 98% and 86% when determined from photos and about 88% and 76% when determined from MR images. The displacement between the centers of the necrotic lesion formed and planned for treatment was about 1 mm in the focal plane and about 2 mm in the axial plane. Our ablation device can be used as an effective and safe tool to plan, monitor and treat solid tumors in small animals and to test new anti-cancer drugs in preclinical studies.

1. Introduction

Imaging-guided HIFU ablation technique is increasingly used in clinical practice for the treatment of solid tumors due to its non-invasive nature (no surgical intervention), lack of ionization, the ability to repeat treatment and minimal side effects, as compared to conventional cancer treatment methods (e.g. radio- or chemotherapy, surgery) [1]. For image-guided HIFU ablation systems, the accuracy of targeting the HIFU beam focus on the treated volume inside the tissue is critical to the safety of healthy tissues surrounding the tumor [2]. In order to deliver the appropriate energy - concentrated in the focal volume of the HIFU beam - to the local volume inside tissue planned for treatment, as well as in order to plan and monitor the treatment, B-mode ultrasound imaging (USI) or magnetic resonance imaging (MRI) is used [3]. The advantage of MRI-gHIFU systems is better image resolution and the ability to monitor temperature maps in the targeted area [4,5]. However, the duration of the treatment procedure using those systems is much longer than that when using USI-gHIFU systems. In addition, the price and operating costs of MRI-gHIFU systems are much higher than those controlled by ultrasound imaging [6]. An advantage of USI-gHIFU systems is the ability to monitor the treatment in real-time.

Bowl-shaped phased-array HIFU transducers have become a standard component in most commercial imaging-guided HIFU ablation devices because they allow electronic control of the HIFU beam focus position and simultaneous generation of multi-focal beams, which reduces treatment time [7]. However, such multi-element probes are much more expensive than

* Corresponding author at: IPPT PAN, Pawińskiego 5b, 02-106 Warsaw, Poland.
E-mail address: tkujaw@ippt.pan.pl (T. Kujawska).

https://doi.org/10.1016/j.apacoust.2021.108367
0003-682X/

single-element probes, and their excitation requires extensive multi-channel electronics. This leads to further increase in price of such imaging-guided HIFU ablative devices. The information obtained from B-mode ultrasound images is two-dimensional, while the phased-array HIFU transducer allows to adjust the position of the HIFU beam focus in 3D space. This makes it difficult to control the HIFU beam focus on image and to plan and monitor treatment. A simple solution to this problem is to replace the B-mode imaging probe with a volumetric one. Such a solution ensures accuracy and reliability, but is quite expensive and increases the complexity of the device [8]. Another solution is to track the electronically controlled focus of the HIFU beam on ultrasound images obtained using B-mode imaging probe rotated around its axis with a selected step by means of a special rotating platform [9]. This approach is also complicated and quite expensive.

Our goal was to design and build a low-cost robotic USI-gHIFU ablative device, ensuring the stability and accuracy of positioning of the HIFU beam focus, and then to estimate its targeting accuracy to support the planning, real-time monitoring and treatment of solid tumors implanted in small animals.

Before assessing the safety and efficacy of our experimental system on animals, an assessment of its targeting accuracy is required. Most published methods for assessing the accuracy of targeting of the existing HIFU ablation systems relate to those guided by MRI [10–12]. There are only a few publications on the accuracy of targeting of HIFU ablative devices guided by ultrasound imaging [9,13,14]. Since the size of the tumor planned to be treated is much larger than the size of the focal volume of the HIFU beam, precision positioning of the HIFU focus in the nodes of the spatial grid covering the tumor is required to ensure thermal destruction of the entire tumor. To ensure the stability and accuracy of targeting, the existing HIFU ablation systems are connected with a robotic arm whose positioning errors were found to be within 0.5 mm [15–17]. However their accuracy of targeting published so far concern only HIFU beam focal plane [9,13]. In this study, we assess the accuracy of targeting of our device both in the axial and focal planes of the HIFU beam.

We have developed, designed and built a low-cost, compact robotic USI-gHIFU ablative device for preclinical trials on small animals. Our device integrates the HIFU ablative system, ultrasound imaging system, computer-controlled precise positioning system and computer with custom software. Before this device is used to treat animals, a number of studies on *ex vivo* tissues were needed to evaluate the accuracy of its targeting. The objective of these studies was to evaluate experimentally the accuracy of targeting of our device using *ex vivo* pork loin samples embedded in a cylindrical reference chamber. The volume to be treated was pre-determined to be a cylinder much smaller than the chamber and coaxially located at a selected depth below the tissue surface. The ultrasound imaging probe was mounted coaxially with the HIFU transducer in its central hole. Therefore, the HIFU beam focus has always been on the central axis of the ultrasound image of the tissue chamber at a selected depth below the tissue surface. The developed device allowed the mechanical movement of the tissue chamber in both, the parallel and perpendicular directions to the imaging plane. This provided the ability to outline the treated area on the axial B-mode image of the tissue chamber and to plan the treatment by programming the targeted ablation volume. The appearance of a hyper-echoic area on the central axis of the axial ultrasound image was an indicator of successful ablation. The cross-sections of the created necrotic lesion visualized after sonication were compared with those planned for treatment.

2. Materials and methods

2.1. USI-gHIFU experimental setup

As mentioned above, our ablative device integrated the following units: USI-gHIFU system, HIFU driving system, diagnostic ultrasound scanner, 4D positioning control system and computer with custom software as a user interface console. Block-diagram of our device is shown in Fig. 1.

The USI-gHIFU system included a single-element bowl-shaped H102 HIFU probe (Sonic Concepts Inc, Bothell, WA, USA) integrated coaxially with a Zonare P10-4 imaging probe mounted in its 20-mm central hole and connected with a Zonare ultrasound scanner (Zonare Medical Systems Inc., Mountain View, CA, USA). The HIFU transducer with an effective diameter of 64 mm and focal length of 62.6 mm could operate at a 1.08 MHz or 3.21 MHz frequency. The USI-gHIFU system was mounted in the bottom of the water tank. In order to excite the HIFU transducer with electric sinusoidal pulses of the selected amplitude, duration and duty-factor, the electronic system including an Agilent 33250A function generator (Colorado Springs, USA) and ENI 3100LA power amplifier (55 dB) (Rochester, New York, USA) was used. To ensure that the same number of pulses was delivered to each ablated tissue volume induced by a single 3-second sonication, the AFG 3102 function generator (Tektronix Inc., Beaverton, OR USA) was used. The waveforms of generated pulses were displayed using an MSO6052A mixed signal oscilloscope (Agilent Technologies, Santa Clara, CA USA). The amplifier output signal excited the HIFU transducer to produce the pulsed HIFU beam with an average acoustic power of 108 W, pulse duration of 0.3 s and duty-factor of 0.6. The values of these parameters result from the HIFU beam properties optimization described in our previous publications [18,19]. The voltage applied to the transducer was 371 V_{pp}. The average acoustic power for the beams used was measured using an UPM-DT-1E ultrasound power meter (Ohmic Instruments, St. Charles, MO, USA).

Above the USI-gHIFU system, at a selected distance from it, there was a frame - with a removable plate for placing an animal or tissue chamber - connected to a slider of the mechanical system of its precise positioning both in the *x*, *y*, *z* directions and at the selected angle of inclination. During experiments with the *ex vivo* tissue samples, this angle was 0°. The precise positioning system was located on the top of the water tank. The removable plate had a circular hole - located coaxially with the integrated heating and imaging probes through which the HIFU beam penetrated the animal body/tissue sample, concentrating its energy in a small volume (focal volume of the HIFU beam) and inducing an increase in temperature leading to local coagulation necrosis. Due to the coaxiality of the imaging and HIFU probes, the focus of the HIFU beam in the initial position was always located on the central axis of the B-mode image of the axial section of the tissue chamber at a selected depth resulting from the geometry of the HIFU transducer and the two-layer media of propagation: water - tissue. The development of the treatment plan consisted in selecting the targeted area on the axial B-mode image and programming the movement of the tissue chamber in the *xy* plane, perpendicular to the ultrasound imaging plane (*xz*), ensuring necrosis covering the entire intended cylindrical volume inside the tissue without damaging the surrounding structures. The appearance of a hyper-echoic area on the axial B-mode image was considered as an indicator of successful ablation. The scanning of the entire targeted tissue volume by the HIFU beam focus was performed automatically using the positioning control system after programming the trajectory of the slider movement and the time and distance intervals between exposures. The movement of the slider was computer-controlled *via* the custom software with input parameters determined from

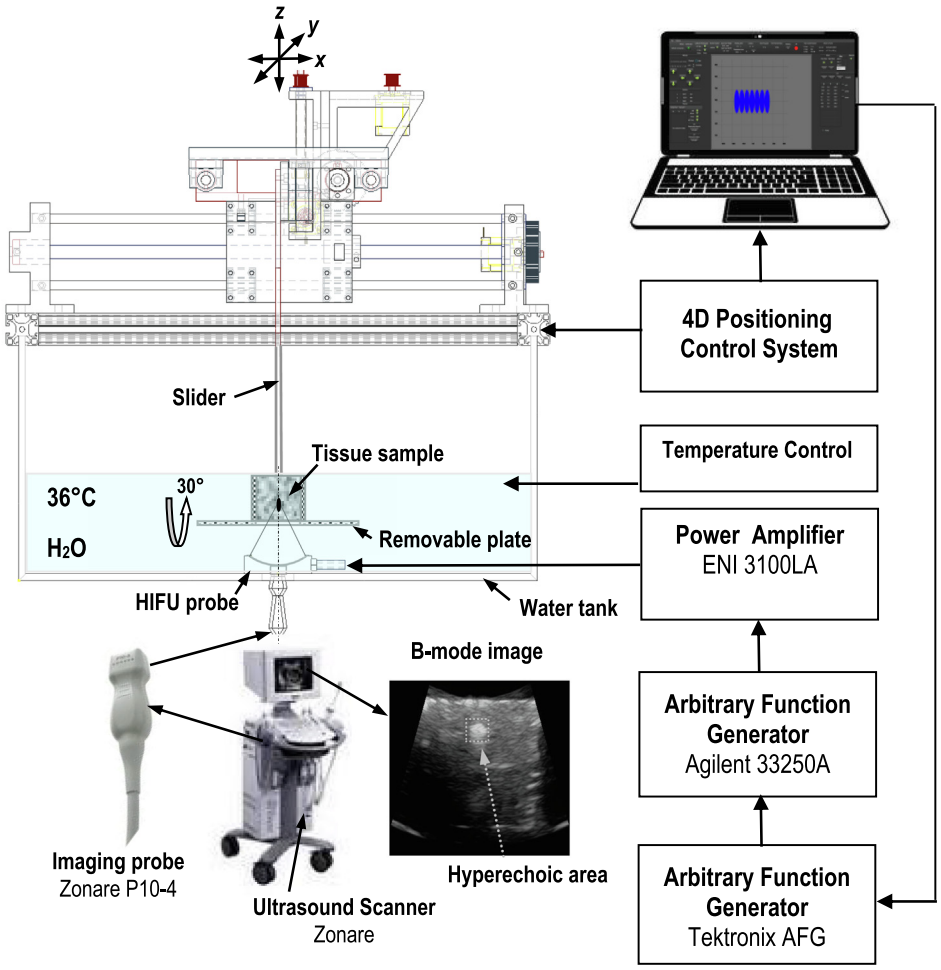

Fig. 1. Block-diagram of the experimental setup for creating necrotic lesions inside *ex vivo* tissue samples by HIFU beams.

the location and size of the necrotic lesions formed in the examined tissue after its single exposures and visualized by various imaging methods [19].

Prior to ablation of the entire intended volume inside the tissue, a B-mode image of the axial section of the cylindrical tissue chamber was recorded. This allowed for the treatment planning by programming the coordinates of the volume planned for ablation and its center, as well as for the identification of the necrotic lesion formed after sonication. The appearance of a hyper-echoic area on the central axis of the axial ultrasound image of the tissue after several sonications in its initial position was considered as an indicator of hitting the center of the planned ablation volume. Axial and radial sections of each necrotic lesion formed after sonication were compared with those planned for treatment by visualizing them using ultrasound imaging, magnetic resonance imaging, and photos taken after cutting each sample along or across its axis.

As was mentioned above the design of our ablative device provided the initial position of the tissue chamber coaxially with both, the HIFU and ultrasound imaging probes. The axial distance between the HIFU transducer and tissue surface was determined from the non-linear propagation model [20] in water as the axial distance from the HIFU transducer, at which the amplitude of the second harmonic begins to rise rapidly. For the transducer used this distance amounted to 50 mm. Then each HIFU beam was focused inside the tissue at a depth of 12.6 mm below its surface. The tissue chamber was immersed in water. The temperature of the water was controlled using an Aquael 100 electric heater (Aquael Sp. z o.o. Warsaw, Poland) placed in the water tank. All experiments were carried out at the 36 °C temperature of the tissue and water. Fig. 2 illustrates the two-layer media of propagation containing a layer of water (50 mm) and tissue (40 mm).

In order to rationally use tissue samples and to maximize the collected statistical data from measurements, each sample was sonicated on both sides.

2.2. Preparation of tissue samples

Tissue samples were prepared from *ex vivo* pork loin pieces. They were cut with a cylindrical knife into blocks, then degassed and inserted into a cylindrical reference chamber with an internal diameter of 43.5 mm and height of 40 mm. To prevent the water - tissue surface from folding, the chamber had sound-transparent windows made of 20-μm thick Mylar film stretched tightly at each its end.

2.3. Ablation planning

As mentioned above, the ablation plan was prepared from the ultrasound images of the axial and radial cross-sections of the reference tissue chamber, made before sonication. In the initial central position of the HIFU beam, the central axis of the ultrasound image overlaps the axis of the cylindrical chamber. Therefore, the focal spot of the HIFU beam in this position is always on the central axis of the B-mode image at a selected depth below the tissue

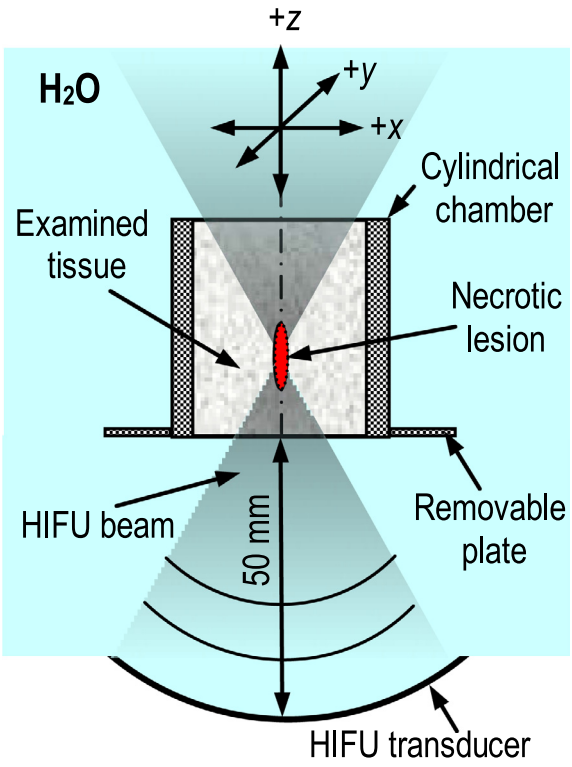

Fig. 2. Scheme of the two-layer media of propagation for the HIFU beam.

surface. The indicator of hitting the target with ablation was the appearance of the hyper-echoic area on the central axis of the ultrasound image after several central sonications.

The treatment plane in the form of a concentric circle in the beam focal plane and a rectangle in the axial plane was made on ultrasound images of both, the axial and radial cross-sections of the tissue chamber, as shown in Fig. 3.

The center of the chamber was determined and marked as the intersection of the two diagonals of the square circumscribed on the circle of the radial section of the chamber. The targeted tissue volume planned for ablation was a coaxial cylinder with a given diameter, much smaller than the inner diameter of the chamber. The center of this cylinder was located on the axis of the tissue chamber at a depth of 12.6 mm below the tissue surface.

According to the results of the experiments published in our previous work [19], the length of the ellipsoidal necrotic lesion created in the examined tissue by a single HIFU beam with acoustic parameters used here was about 10.3 mm and a diameter of about 1.9 mm for 1.08 MHz beams. For 3.21 MHz beams, these values were about 5.2 mm and 1.7 mm, respectively.

To cover the entire tissue volume planned for treatment with necrosis, multiple necrotic lesions were created by moving the tissue chamber between exposures along the programmed trajectory with the selected time and distance intervals using a computer-controlled precision positioning system. As mentioned above, 1.08 MHz or 3.21 MHz HIFU beams with 0.3 s pulse duration and 0.6 duty-cycle, propagating in two-layer media: water - tissue (50 mm – 40 mm) were used. The duration of a single exposure with the same number of pulses was 3 s.

Four cylindrical volumes of different diameters (5 mm and 9 mm for 1.08-MHz HIFU beams as well as 5 mm and 8 mm for 3.21 MHz beams) centered on the axis of the tissue chamber at a depth of 12.6 mm below the tissue surface were selected for ablation. The positions and sequence of individual ablations - in the focal plane of the HIFU beam used - in order to create a necrotic lesion of a selected size are shown in Fig. 4.

For each HIFU beam with a selected frequency, two cylindrical necrotic lesions of a selected diameter were created, one on each side of the tissue sample. A 2-minute cooling time intervals between exposures, resulting from the tissue relaxation time, was applied to minimize the effect of a secondary temperature, remaining at the site of the previous ablation, on the extent of the lesion induced by the neighboring ablation. Additionally, for the same purpose, the trajectory of the beam motion was selected in such a way as to maximize the distance between consecutive exposures.

After sonication, the axial and focal cross-sections of created necrotic lesions were compared with those intended for treatment using various methods of their visualization (ultrasound, magnetic resonance and optical imaging). The displacement between them was assessed. Comparison was done for each tissue volume planned for treatment.

2.4. Ultrasound imaging

After sonication, the ultrasound images of the axial and radial cross-sections of each necrotic lesion created inside the tissue sample were recorded. The hyper-echoic area on the B-mode image was identified and analyzed in terms of its location and size.

2.5. MR imaging

After sonication, the necrotic lesion formed in each tissue sample was visualized by MR imaging using Bruker Biospec 70/30USR magnetic resonance scanner with 7 T induction of magnetic field

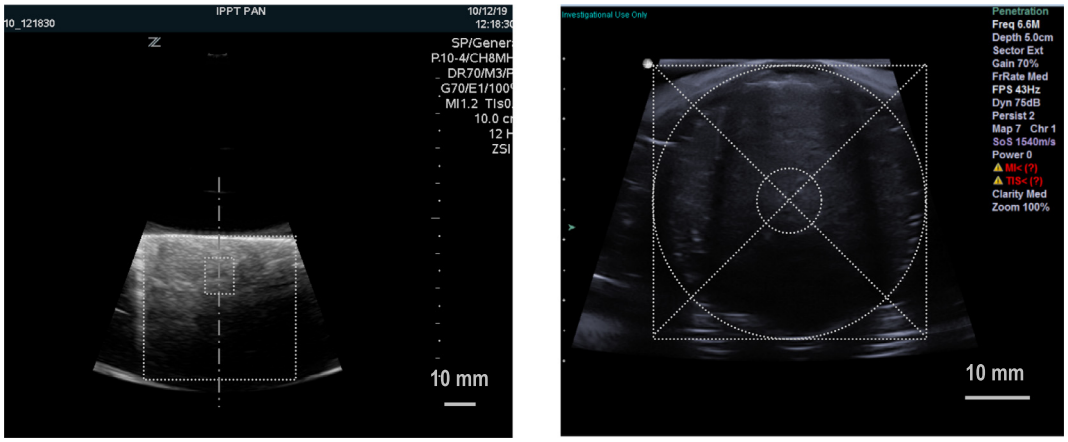

Fig. 3. Ultrasound image of the axial (left) and radial (right) cross-section of the tissue chamber. The inner rectangle and circle indicate the targeted area corresponding to the axial and radial cross-section of the 9 mm tissue volume planned for ablation by 1.08-MHz HIFU beams.

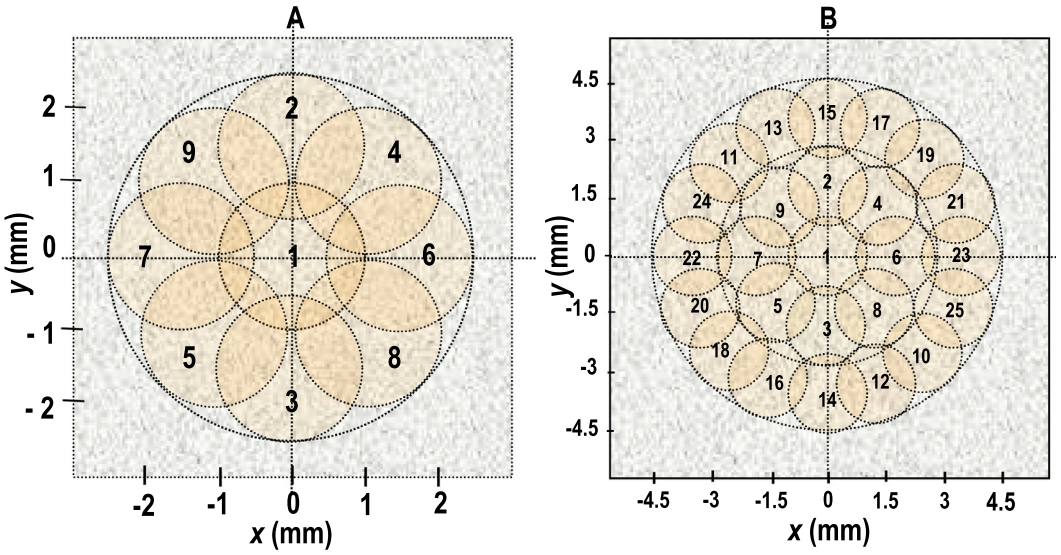

Fig. 4. Positions and sequence of the individual ablations to create a 5-mm (A)) and 9-mm (B) cylindrical necrotic lesion by 1.08-MHz beams.

(Bruker Polska Sp. z o.o., Poznań, Poland) and analyzed. The MR images obtained were pre-processed with OsiriX Lite software (Pixmeo SARL, Switzerland) to create a single image with minimum-intensity projection (MinIP) area (corresponding to the necrotic lesion) from the sequence of MR images covering the entire volume of the lesion. The extent and location of each lesion was assessed with the ImageJ software [21] and Matlab toolboxes (MathWorks Inc., Natick, MA, USA) using a single MR image created after processing all sliced images by means of the Minimum Intensity Projection (MinIP) method. This allowed firstly to rescale each image (by specifying the number of pixels in 1 mm of the real scale), and then to determine the center of the planned necrosis and the average value of the brightness intensity both in the area of the necrotic lesion and the surrounding tissue. The obtained values allowed to normalize the brightness intensity in grayscale for each image. Then the section of the created lesion was moved to the center of the section planned for ablation. This made it possible to obtain information about the displacement between them and to assess the accuracy of targeting for our device.

Percentages determining what part of the cross-sectional area of the tissue volume planned for ablation was not covered with necrosis (α), what part of the cross-sectional area of the created lesion exceeds the area planned for ablation (β), and what part of the cross-sectional area of the tissue volume planned for ablation was covered with necrosis (γ), were calculated from the following formulas:

$$\alpha = \frac{S(P\bar{C})}{S(P)}100\%, \tag{1}$$

$$\beta = \frac{S(C\bar{P})}{S(C)}100\%, \tag{2}$$

$$\gamma = \frac{S(P \cap C)}{S(P)}100\%. \tag{3}$$

where S is the axial or radial cross-sectional area, P is a set of pixels in the section of the tissue volume planned for ablation and C is a set of pixels in the section of the necrotic lesion created.

2.6. Optical imaging

After visualization of the created lesions using the ultrasound and magnetic resonance imaging, each tissue chamber was frozen for about 2 h at the temperature of –18 °C. Next, each hardened tissue sample was removed from the chamber and sectioned to make the necrotic lesions visible at their axial or radial (in the focal plane) sections. The location and extent of each lesion was assessed from grayscale-converted photographs processed using the same methods as for MR images. Percentages α, β and γ were calculated from the formulas (1), (2) and (3), respectively.

2.7. Statistical analysis of results

As mentioned above, to maximize the use of each tissue sample and the amount of statistical data collected, each sample was sonicated on both sides. 9 exposures were used to create a cylindrical necrotic lesion with a diameter of 5 mm by 1.08-MHz HIFU beams (Fig. 4A) and 13 exposures when using 3.21-MHz beams. In order to create a 9-mm lesion by 1.08-MHz HIFU beams 25 exposures (Fig. 4B) were used. For 3.21 MHz beams a 8-mm lesion was formed using 33 sonications. Two samples were used in the experiments with HIFU beams of the same frequency to create a cylindrical lesion of the same diameter. In total, 16 lesions were included in the experiments. The mean value of the position of the center of the necrotic lesions and their size was determined along with the standard deviations.

3. Results and discussion

The targeting accuracy of our robotic USI-gHIFU ablative device in the axial and focal planes was evaluated experimentally using various methods of visualizing necrotic lesions formed inside the pork loin tissue *ex vivo* after its multiple sonications by a HIFU beam moved with a selected step along a programmed trajectory leading to necrosis the entire treated volume inside the tissue. Then the visualized sections of the necrotic lesions formed were compared with those planned for treatment.

Fig. 5 shows exemplary photos of a radial section of a necrotic lesion of different diameter, formed in an *ex vivo* pork loin tissue sample by a HIFU beam of the same frequency. Photos were taken after cutting the frozen sample in the focal plane of the HIFU beam. Sample photos of the axial section of these lesions are shown in Fig. 6.

As can be seen from the above photos, each necrotic lesion was easy to detect due to the clearly outlined boundary between the necrotic tissue and the surrounding non-discolored tissue. The

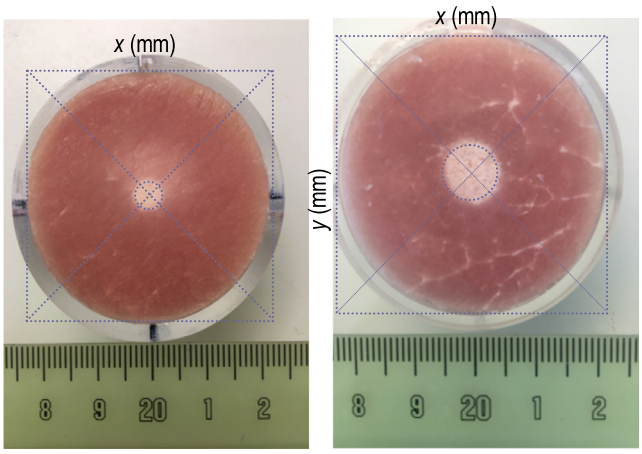

Fig. 5. Photos of the radial section of a 5-mm (left) and 9-mm (right) cylindrical necrotic lesion formed in the examined tissue by the 1.08 MHz HIFU beams.

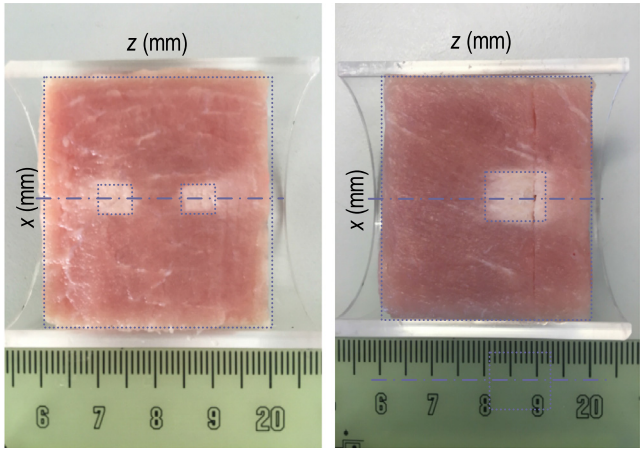

Fig. 6. Photos of the axial section of a 5 mm (left) and 9 mm (right) cylindrical necrotic lesion formed in the examined tissue by the 3.21-MHz HIFU beams on both sides (left) and 1.08-MHz HIFU beams on one side (right), respectively.

location and size of the tissue volume planned for treatment in the radial section photos was marked as a circle of a given diameter with the center at the intersection of the diagonals of the square circumscribed on the circle with a diameter equal to the inner diameter of the tissue chamber. In the photos of the axial sections of the tissue area planned for ablation was marked as a rectangle with sides equal to the diameter and length of the planned cylindrical necrotic volume. The center of the rectangle was on the axis of the chamber at 12.6 mm below the tissue surface. Therefore, on the basis of cross-sectional photos of the necrotic lesion, its location, size and displacement in relation to the lesion planned for treatment were determined.

In Fig. 7 exemplary MR images of the radial section of the necrotic lesion of various diameter formed in the tested tissue by the HIFU beams with given acoustic properties are displayed. This figure shows the MR images from the focal plane of the HIFU beam. The area of the necrotic lesion planned to be treated is displayed as a circle, the area created is shown as a dark region. Exemplary MR images of the axial cross-section of the created lesions are shown in Fig. 8.

Fig. 9 shows how the size of the hyper-echoic area on the ultrasound image of the axial section of the tissue sample increases with the increase in the number of sonications needed to create a necrotic lesion of the intended diameter by the applied HIFU beam. As can be seen from this figure, the hyper-echoic area first appeared in the center of the pre-determined targeted area planned for ablation and marked with a rectangle. The appearance of this area directly confirmed the formation of a necrotic lesion on the axis of the tissue chamber at a given depth. However, after sonication of the entire intended volume inside the tissue sample, it was difficult to assess the extent of the necrotic lesion formed from the obtained ultrasound images of its cross-sections due to their indistinctly outlined boundaries.

Fig. 10 presents exemplary ultrasound images of the radial section of the examined tissue sample before, during and after sonication by the HIFU beam of a given frequency, leading to the formation of a cylindrical necrotic lesion of the planned diameter. As can be seen from these images, the necrotic lesion was formed in the right place, in the center of the marked area, however, on the basis of these images, it was difficult to clearly determine its size due to the blurred boundaries of the hyper-echoic area.

The obtained results showed that the necrotic lesions induced inside the examined tissue by the HIFU beams used arises exactly in the targeted tissue volume predetermined on the ultrasound images and marked with a circle or rectangle. The accuracy of targeting of our device was evaluated by the ratios α, β and γ calculated from photos and MR images and specified in Table 1 and Table 2, respectively.

Fig. 11 shows the exemplary contours of the cross-sectional area of the necrotic lesion planned for ablation and that created inside the tested tissue sample after its sonication by HIFU beams of the given frequency.

The circle and jagged contours reflecting cross-sectional boundaries of the treated tissue volume outlined the area planned for ablation and that created, respectively. The cross-sectional area of the tissue volume planned for ablation and created as well as the displacement between their centers and the maximum exceeding of the lesion borders outside or inside the planned area was calculated from the photos and MR images and are presented in Table 1 and Table 2, respectively.

According to the results presented in Table 1 and Table 2, the mean ratio of the cross-sectional area of the tissue volume covered with necrosis to that planned for ablation (γ) was approximately 97.95% when determined from the photos and approximately 87.6% when determined from the MR images. The mean ratio of the axial section area of the tissue volume covered with necrosis to that planned for ablation was about 86.2% when calculated from the photos and about 76.1% when calculated from the MR images. The mean value of the displacement between the centers of the radial sections was found to be about 1 mm when calculated from the photos and about 0.74 mm when determined from the MR images. The mean value of the displacement between the centers of the axial sections was found to be about 1.38 mm and 1.08 mm when calculated from the photos and MR images, respectively. The obtained values indicate that both the size and location of the created lesions agree fairly well with those planned for treatment. The mean value of the ratio determining what fraction of the necrotic lesion formed exceeds the boundaries planned for ablation (β) amounted to about 18.47% and 7.8% for the radial sections and 17.07% and 8.8% for the axial sections when calculated from the photos and the MR images, respectively. The mean value of the ratio determining what fraction of the necrotic lesion planned for ablation was not covered with necrosis (α) was about 2.25% and 12.4% for the radial sections and 13.8% and 23.9% for the axial sections when calculated from the photos and MR images, respectively.

In clinical practice, a 10-mm margin around the tumor contour is usually assumed to ensure treatment safety [1]. In our experiments, the maximum exceeding of the necrotic lesion beyond the

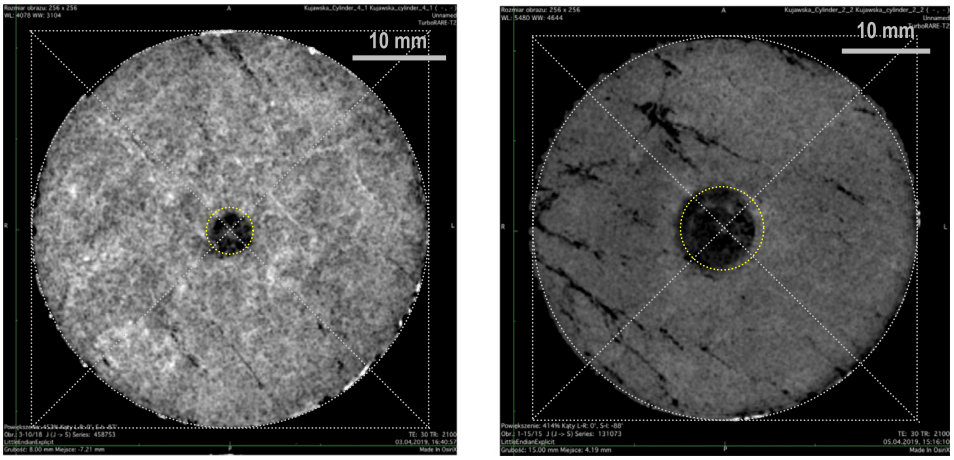

Fig. 7. T1-weighted MR image of the focal cross-section of a 5-mm and 9-mm cylindrical necrotic lesion created by 3.21-MHz (left) and 1.08-MHz (right) HIFU beams, respectively.

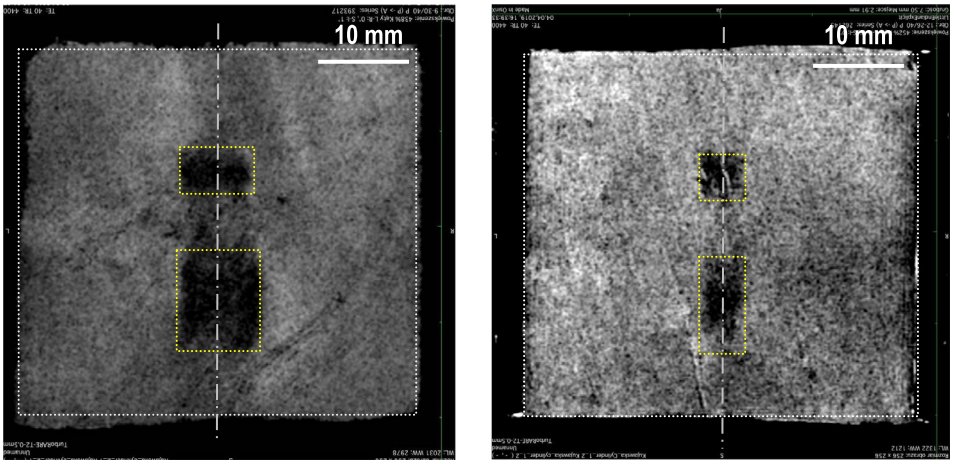

Fig. 8. T1-weighted MR images of the axial cross-sections of the 9 mm and 8 mm (left) as well as 5 mm (right) necrotic lesions created in the tissue sample respectively by 1.08-MHz (bottom lesions) and 3.21-MHz (top lesions) HIFU beams, respectively.

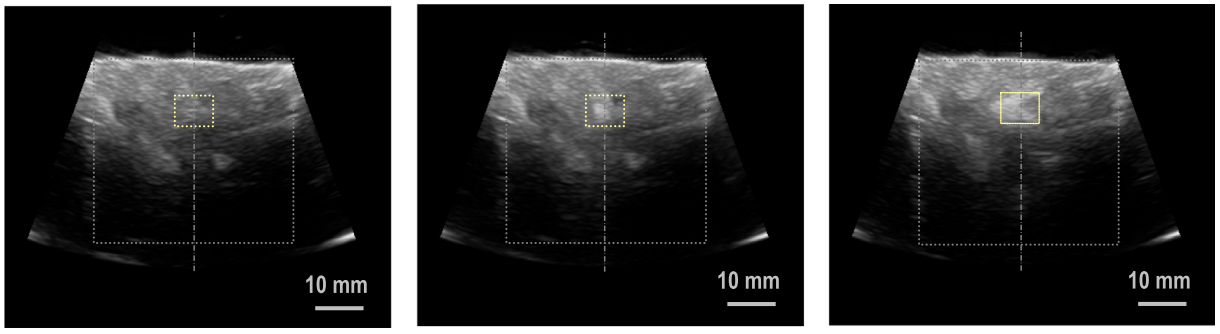

Fig. 9. Ultrasound image of the axial section of a tissue sample before (left), during - after 3 central exposures - (center) and after sonication (right) by 3.21-MHz HIFU beams leading to necrosis covering the entire 8-mm cylindrical volume inside the tissue.

boundaries of the tissue volume planned for treatment was less than 2 mm, when determined from the cross-sectional images which meets the requirements for the use of our ablation device in preclinical trials on small animals.

The obtained results showed that our robotic ablative device is capable of creating necrotic lesions exactly in the targeted tissue volume, intended for the treatment and determined on the ultrasound images before the therapy. According to the data presented in Table 1 and Table 2, its accuracy of targeting was about 2 mm in the B-mode imaging plane and about 1 mm in the focal plane of the HIFU beam used, which is comparable to the accuracy of targeting of other imaging-guided HIFU ablative devices [11,22]. Therefore, our device guided by ultrasound imaging can be used as an effective tool for planning, monitoring and conducting thermal

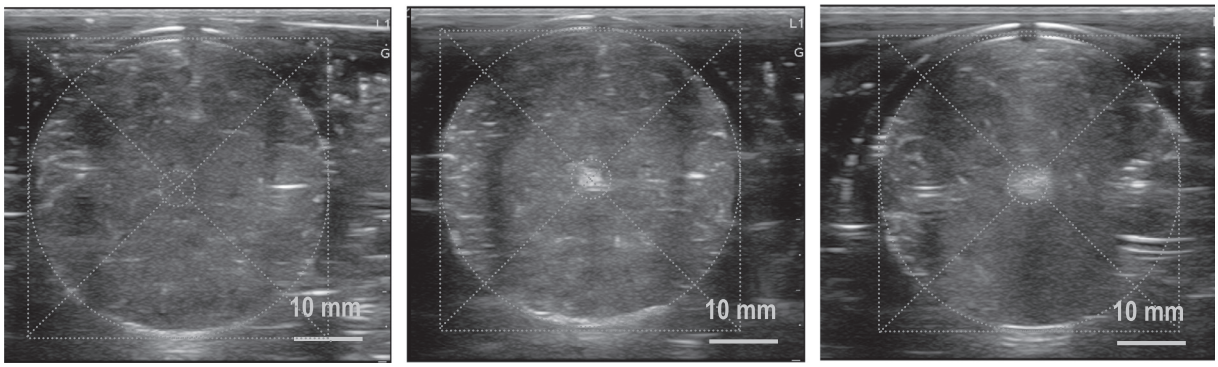

Fig. 10. Ultrasound image of a focal cross-section of a tissue sample before (left), during - after 3 central exposures - (center), and after sonication (right) by 1.08-MHz HIFU beams leading to necrosis covering the entire 5-mm cylindrical volume inside the tissue. The images show tissue cross-sections in the focal plane of the HIFU beams.

Table 1
Mean value and standard deviation of the size of the necrotic lesion formed and planned for ablation and displacement between their centers when calculated from photos.

	Mean ± standard deviation	
	Radial section area	Axial section area
Displacement between centers Δl [mm]	1.01 ± 0.18	1.38 ± 0.37
α [%]	2.25 ± 2.01	13.80 ± 2.69
β [%]	18.47 ± 9.55	17.07 ± 5.49
γ [%]	97.75 ± 2.01	86.20 ± 2.69

Table 2
Mean value and standard deviation of the size of the necrotic lesion formed and planned for ablation and displacement between their centers when calculated from MR images.

	Mean ± standard deviation	
	Radial section area	Axial section area
Displacement between centers Δl [mm]	0.74 ± 0.59	1.08 ± 0.26
α [%]	12.4 ± 6.4	23.9 ± 4.2
β [%]	7.8 ± 4.2	8.8 ± 2.0
γ [%]	87.6 ± 6.4	76.1 ± 4.2

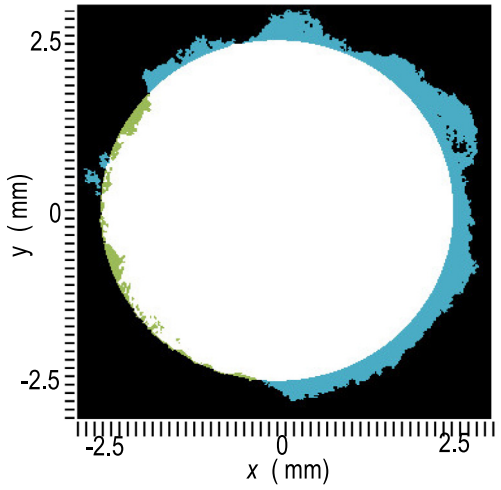

Fig. 11. A binary cross-sectional map of a 5-mm necrotic lesion, appropriately planned for ablation (circle boundaries) and formed (jagged boundaries) inside the tissue sample after its multiple sonications by the 3.21-MHz HIFU beam. Necrosis extending outside the circle is colored blue, and the area inside the circle not covered by necrosis is green. (For interpretation of the references to colour in this figure legend, the reader is referred to the web version of this article.)

damage to solid tumors in small animals. We have proved that the treatment planning with our device, consisting in recording the B-mode images from treatment planes, selecting the target area on them and programming the trajectory of the HIFU beam movement leading to necrosis covering the entire treated tissue volume is effective.

The assessment of the accuracy of targeting of our device may be affected by errors from the following sources: inaccuracies in the construction of the device or tissue chamber and inaccuracies in measurements. When the errors come from the inaccuracy in the construction of the device, the central axis on the axial B-mode image may be slightly deflected from the axis of the HIFU beam. This can lead to misalignment between the cross-sections of the necrotic lesion planned for treatment and those created. In order to minimize such an error, the device was calibrated (using a hydrophone moved in the plane of the removable plate opening) by mechanically adjusting the position of the HIFU transducer in relation to the imaging probe. During the procedure, the cylindrical chamber containing the tissue sample was moved horizontally (in the *xy* plane) so that its walls (as reference markers) could be easily identified on ultrasound images of its sections in the *yz*-planes parallel to the axial plane. The B-mode image of the tissue sample in the focal plane of the HIFU beam was recorded before and after ablation by means of a linear phased array probe with which the ultrasonic scanner used was equipped. Errors resulting from inaccuracies in measurements and the variety of tissue samples were minimized by repeating the experiments several times. Therefore, the averaged results presented in Table 1 and Table 2 contain a stable and repeatable error characterizing the targeting accuracy of our device.

The size of the tissue volume that can be effectively treated with our device is limited by the size of the animal, the duration of one-time anesthesia and the standards specifying the permissible thermal dose for small animals. It is usually a compromise between the typical duration of anesthesia and the exposure time needed to cover the entire tumor volume with necrosis. The maximum diameter of tumors to be treated with this device is 10 mm. The maximum depth of their seating under the skin is 15 mm. The trajectory of the HIFU beam movement, determining the position and sequence of individual exposures (see Fig. 5), was selected to minimize the effect of the secondary temperature increase induced in the tissue at the site of the next sonication by the previous ablation, when the time interval between exposures is shorter than the tissue temperature relaxation time. The experimental results showed that the automated procedure for targeting of the HIFU

beam focus at the intended tissue volume and monitoring local ablation is effective. Nevertheless, the tissue volume subjected to ablation in our experiments was limited to a cylinder with a maximum diameter of 9 mm and a height of approximately 11 mm. This volume resulted from the size of the tumors implanted in the rats planned for treatment (with a maximum diameter of approx. 10 mm) and the maximum possible duration of single anesthesia during therapy, without supplementation that could lead to repositioning of the rat. As with most existing HIFU ablative devices guided by ultrasound imaging, the appearance of a hyperechoic area on the B-mode image was an indicator of successful local ablation of the intended volume inside the treated tissue.

The appearance of a hyper-echoic area on the ultrasound image is conditioned largely on the acoustic intensity level in the focal plane of the HIFU beam used. The average acoustic power of the 1.08 MHz and 3.21 MHz HIFU beams used generated in water was 108 W and 51.3 W, respectively. In our experiments, the HIFU beams were propagated in a two-layer system of media: water - tissue (50 mm – 40 mm). The focal I_{SATA} intensity of the applied HIFU beams inside the examined tissue was calculated using the k-Wave non-linear propagation model described in [20] and was equal to 9.6 kW/cm^2 and 17.7 kW/cm^2 for 1.08 MHz and 3.21 MHz beams, respectively.

4. Conclusions

The obtained results of our experiments proved that the reference cylindrical chamber containing the sample of the *ex vivo* tissue examined is suitable for assessing the accuracy of targeting of our robotic ultrasound imaging-guided HIFU ablative device. The targeting accuracy of our device was found to be about 2 mm in the imaging plane and about 1 mm in the focal plane of the HIFU beam. These values are within the 10-mm margins assumed in clinical practice for therapeutic safety and are comparable to the targeting accuracy of other imaging-guided HIFU ablation devices. Therefore, our robotic HIFU ablation device can be useful in preclinical studies for planning, monitoring and ablating solid tumors implanted in small animals, as well as for testing novel anticancer drugs. Our future research will focus on the use of our HIFU device both for the ablative treatment of solid tumors implanted in small animals and for the development of a new treatment strategy based on tumor hyperthermia induced by ultra-short, time-fractionated Low-Intensity Focused Ultrasound and combined with the delivery of a test cytotoxic drug in thermo-sensitive liposomal carriers.

In addition, the basic advantage of the developed device, especially over devices guided by MR imaging, is its simple and easy-to-use design, as well as low manufacturing and operating costs.

Declaration of Competing Interest

The authors declare that they have no known competing financial interests or personal relationships that could have appeared to influence the work reported in this paper.

Acknowledgments

This work was supported by the National Science Centre under Grant 2016/21/B/ST8/02445 and by the ESF, POWR.03.02.00-00-I028/17-00.

References

[1] Zhou Y-F. High intensity focused ultrasound in clinical tumor ablation. World J Clin Oncol 2011;2(1):8. https://doi.org/10.5306/wjco.v2.i1.8.
[2] ter Haar G. Safety first: progress in calibrating high-intensity focused ultrasound treatments. Imaging Med 2013;5(6):567–75.
[3] Ebbini ES, Ter Haar G. Ultrasound-guided therapeutic focused ultrasound: current status and future directions. Int J Hyperthermia 2015;31(2):77–89.
[4] Zhang L et al. Feasibility of magnetic resonance imaging-guided high intensity focused ultrasound therapy for ablating uterine *fibroids* in patients with bowel lies anterior to uterus. European J Radiol 2010;73:396–403.
[5] Tempany CMC, Stewart EA, McDannold N, Quade BJ, Jolesz FA, Hynynen K. MR imaging-guided focused ultrasound surgery of uterine leiomyomas: a feasibility study. Radiology 2003;226(3):897–905.
[6] Zhang L, Orsi F, Arnone P, Chen W. High intensity focused ultrasound ablation: a new therapeutic option for solid tumors. J Cancer Res Therap 2010;6(4):414. https://doi.org/10.4103/0973-1482.77064.
[7] Fan X, Hynynen K. Ultrasound surgery using multiple sonications - treatment time considerations. Ultrasound Med Biol 1996;22(4):471–82.
[8] Ziadloo A, Vaezy S. Real-time 3D image-guided HIFU therapy. Proc Int Conf IEEE Eng Med Biol Soc 2008:4459–62.
[9] Li K, Bai J, Chen Y, Ji X. Experimental evaluation of targeting accuracy of an ultrasound-guided phased-array high-intensity focused ultrasound system. Appl Acoust 2018;141:19–25.
[10] Chauvet D, Marsac L, Pernot M, Boch A-L, Guillevin R, Salameh N, et al. Targeting accuracy of transcranial magnetic resonance-guided high-intensity focused ultrasound brain therapy: a fresh cadaver model. J Neurosurgery 2013;118(5):1046–52.
[11] Kim Y-S, Trillaud H, Rhim H, Lim HK, Mali W, Voogt M, et al. MR thermometry analysis of sonication accuracy and safety margin of volumetric MR imaging-guided high-intensity focused ultrasound ablation of symptomatic uterine fibroids. Radiology 2012;265(2):627–37.
[12] Ellens NPK, Kobelevskiy I, Chau A, Waspe AC, Staruch RM, Chopra R, et al. The targeting accuracy of a preclinical MRI-guided focused ultrasound system. Med Phys 2015;42(1):430–9.
[13] An CY, Syu JH, Tseng CS, Chang C-J. An ultrasound imaging-guided robotic HIFU ablation experimental system and accuracy evaluations. Appl Bionics Biomech 2017;2017:1–8.
[14] Tang T, Azuma T, Iwahashi T, Takeuchi H, Kobayashi E, Sakuma I. A high-precision US-guided robot-assisted HIFU treatment system for breast cancer. Engineering 2018;4(5):702–13.
[15] Chauhan S, ter Haar G. FUSBOTs: empirical studies using a surgical robotic system for urological applications. Proc Int Symp Ther Ultrasound 2007;911:117–21.
[16] Masamune K, Kurima I, Kuwana K, Yamashita H, Chiba T, Dohi T. HIFU positioning robot for less-invasive fetal treatment. Procedia CIRP 2013;5:286–9.
[17] Tseng C, Syu J, An C, Chang C. An ultrasonography assisted robotic HIFU ablation experimental system. Proc Int Conf Biomed Electronics Devices 2015;1:109–14.
[18] Fura Ł, Kujawska T. Selection of exposure parameters for a HIFU ablation system using an array of thermocouples and numerical simulations. Archiv Acoustics 2019;44:349–55.
[19] Fura Ł, Dera W, Dziekoński C, Świątkiewicz M, Kujawska T. Experimental assessment of the impact of sonication parameters on necrotic lesions induced in tissues by HIFU ablative device for preclinical studies. Archiv Acoustics 2021;46(1):1–12.
[20] Treeby BE, Jaros J, Rendell AP, Cox BT. Modeling nonlinear ultrasound propagation in heterogeneous media with power law absorption using a k-space pseudo-spectral method. J Acoust Soc Am 2012;131:4324–36.
[21] Schneider CA, Rasband WS, Eliceiri KW. NIH Image to ImageJ: 25 years of image analysis. Nat Methods 2012;9(7):671–5.
[22] Choi JW, Lee JY, Hwang EJ, Hwang I, Woo S, Lee CJ, et al. Portable high-intensity focused ultrasound system with 3D electronic steering, real-time cavitation monitoring, and 3D image reconstruction algorithms: a preclinical study in pigs. Ultrasonography 2014;33(3):191–9.